Experimental investigations of comparative performance, emission and combustion characteristics of a cottonseed biodiesel-fueled four-stroke locomotive diesel engine

Anirudh Gautam and Avinash Kumar Agarwal

International Journal of Engine Research 2013 14: 354 originally published online 4 September 2012
DOI: 10.1177/1468087412458215

International Journal of ENGINE RESEARCH

Original Article

International J of Engine Research
14(4) 354–372

DOI: 10.1177/1468087412458215
jer.sagepub.com
SAGE

Experimental investigations of comparative performance, emission and combustion characteristics of a cottonseed biodiesel-fueled four-stroke locomotive diesel engine

Anirudh Gautam[1,2] and Avinash Kumar Agarwal[1]

Abstract

A large-bore, four-stroke, medium-speed, compression-ignition railway traction locomotive engine was fueled with cottonseed methyl ester (Biodiesel). The cottonseed methyl ester was stored for 6 months under ordinary storage conditions, and various fuel properties of this seasoned cottonseed methyl ester were evaluated. Various blends of cottonseed methyl ester (B10, B20, B50 and cottonseed methyl ester) were evaluated for engine performance, emissions and combustion characteristics of the locomotive engine compared to baseline diesel. Correlation of the fuel-injection performance parameters with the physical properties of biodiesel has been carried out. The engine was able to operate on cottonseed methyl ester without noticeable power loss. With cottonseed methyl ester, the thermal efficiency decreased marginally by 0.7% and the brake-specific energy consumption increased by 0.1 MJ/kWh at the rated power. Due to the lower calorific value of biodiesel, brake specific fuel consumption (BSFC) increased by 13.4% at eighth engine notch, nitrogen oxide emissions increased by 8% and particulate matter emissions decreased by 32% vis-a-vis mineral diesel. Nitrogen oxide emissions were found to be a function of injection timings, global oxygen/carbon ratios, time of the maximum mean in-cylinder temperatures and apparent heat release. Particulate matter emissions were found to depend on the air–fuel mixture's oxygen/carbon ratio, fuel bound oxygen and fuel-injection pressure. The experiments were carried out to evaluate the in-cylinder pressure, heat-release rate, cumulative heat release, fuel-injection pressure, needle lift and fuel-injection velocities. Increased fuel-injection pressures (1000 bar compared to 900 bar for mineral diesel), advanced fuel-injection timings, shorter combustion duration, advanced in-cylinder pressures and higher heat-release rates were observed for biodiesel and blends. The findings of the present study have provided further insights into the combustion of biodiesel in locomotive engines.

Keywords

Locomotive engine, cottonseed biodiesel, heat-release rate, combustion analysis, performance and emissions.

Date received: 04 September 2011; accepted: 17 July 2012

Introduction

Replacement of mineral diesel with biodiesel for Indian Railways would result in prevention of 1.4 million tons of nitrogen oxide (NO_x) and 0.1 million tons of particulate being emitted into the atmosphere in next 35 years (typical life span of a diesel locomotive). Therefore, there is a desire to substitute diesel traction fuel with renewable fuels like biodiesel from energy security and environmental preservation standpoint. Indian Railways has therefore made an effort to utilize renewable fuels such as biodiesel for this purpose. Diesel locomotives operate in extreme environmental conditions with arduous duty cycles, with a requirement of minimum availability of 99% under all conditions. Introduction of a new fuel, albeit renewable, will also require fulfilling the above operating and reliability requirements. This requires detailed characterization of

[1]Engine Research Laboratory, Department of Mechanical Engineering, Indian Institute of Technology Kanpur, India
[2]Engine Development Directorate, Research Designs and Standards Organisation Lucknow, Ministry of Railways, India

Corresponding author:
Avinash Kumar Agarwal, Engine Research Laboratory, Department of Mechanical Engineering, Indian Institute of Technology Kanpur, Kanpur, India.
Email: akag@iitk.ac.in

Table 1. Technical specifications of the locomotive test engine.

Configuration	V-16, direct-injection, 4S, turbocharged, inter-cooled diesel engine
Bore / stroke (mm)	228.6 / 266.7
Displacement	10.95 liter / cylinder
Compression ratio	11.75 (static)
Fuel injection equipment	Mechanical pump line nozzle system
Nozzle opening pressure	250 bar
Rated power	2312 kW at 1050 r/min
Torque at maximum speed	22,000 Nm at 1050 r/min

the locomotive engine with biodiesel (cottonseed methyl ester (CME) in the present study) and its blends with mineral diesel.

Cottonseeds have approximately 18% (w/w) oil content. India's cottonseed production is estimated to be around 35% of its cotton output (approximately 4.5 million metric tons). Approximately 0.30 million metric ton cottonseed oil is produced in India and it is an attractive biodiesel feedstock. Indian Railway has a fleet of nearly 5000 diesel locomotives, most of which are powered by 16-cylinder, V configuration, four-stroke, diesel engines (DLW, India: ALCO-DLW 251-D) with a rated power output of 2312 kW. The technical specifications of this engine are given in Table 1.

Use of cottonseed oil and its esters as fuel for diesel engines has been investigated by many researchers. Umer et al.[1] obtained fatty acid methyl esters of cottonseed oil by gas chromatography (GC), and ^{1}H nuclear magnetic resonance (NMR) spectroscopy and showed that it consists of methyl esters of five fatty acids: linoleic (53.14%), palmitic (24.90%), oleic (18.93%), stearic (2.63%) and arachidic (0.29%). Nabi et al.[2] reported reduction of CO and particulate matter (PM) emissions with CME in a single-cylinder engine; however, a slight increase in NO_x emissions was reported. CME showed higher kinematic viscosity, density, cetane number and 10% lower calorific value compared to mineral diesel. Rakopoulos et al.[3] investigated performance and emissions of sunflower and cottonseed biodiesel blends (B10 and B20) in a bus engine (six-cylinder, turbocharged, after-cooled, direct-injection (DI) minibus (Mercedes-Benz) diesel engine). They reported lowest soot, highest NO_x, highest total hydrocarbons (THC) and highest brake specific fuel consumption (BSFC) with B20 blend of CME. Agarwal and Dhar[4] evaluated performance, emission and combustion behavior of Jatropha oil blends (unheated) in a direct-injection compression-ignition (DICI) engine. Upon analysis of in-cylinder pressure, heat-release rate and cumulative heat release, they concluded that all test fuels exhibited similar combustion stages as mineral diesel; however, Jatropha oil blends showed earlier start of combustion (SOC) and lower heat-release rates during the premixed combustion phase. THC, CO and NO emissions were found to be slightly higher for higher Jatropha blends. Ben et al.[5] carried out an economic feasibility analysis by developing a complex cost model for cottonseed oil as a biodiesel feedstock. They carried out cost modeling of cottonseed oil biodiesel and performance investigations of CME blends (B2, B5, B10 and B50). The cost model developed by Ben et al.[5] has several interdependent variables such as production capacity, raw material availability, in-plant trucking, storage, operation cost, revenue, depreciation, labor, utilities, capital investment and overhead cost. They assumed an annual production capacity of 10 million gallons of biodiesel with a fixed capital cost and estimated a sale price of US $3.45 per gallon of biodiesel. Conversion efficiency of cottonseeds to CME was taken as 15%. In their model, recovery costs of cottonseed cake, seed hulls, linters and tax incentives have been accounted for. Capareda et al.[6] carried out performance and emission tests with CME in a 14.2 kW diesel engine and showed reduction in THC, NO_x and SO_2 emissions and increase in CO emissions compared to mineral diesel. Savvidis et al.[7] converted cottonseed oil and frying oil to biodiesel and prepared B10, B20, B30, B40, B50 and B100 blends. These blends were used in two cars: Volvo V70 2.5l turbo diesel and Ford Transit 2.5l diesel. They reported decreasing PM emissions with increasing biodiesel content in the test fuel. NO_x emissions were found to be higher with biodiesel blends compared to mineral diesel, and there was an increasing trend of NO_x with increasing biodiesel content in the fuel. However, the architecture of the engine such as combustion chamber design, fuel-injection system, electronic versus mechanical governing had an influence on the NO_x emissions. In another study, Savvidis et al.[8] investigated influence of various CME blends on steady-state emissions using an older technology Ford Escort 1.6l, having four cylinders with an indirect injection (IDI) engine on a chassis dynamometer. The test car was not equipped with an electronic control unit (ECU), and seven test fuels were used (high sulfur diesel, B10, B20, B30, B40, B50 and B100). Fuel-injection timings were kept identical for all test fuels to eliminate injection timing differences for different fuel viscosities and densities. Soot emission decreased for higher CME blends. NO_x emissions increased with increasing engine speeds and with increasing biodiesel content in the test blend.

In summary, various biodiesels including CME, and straight vegetable oils including cotton seed oil and their blends with mineral diesel were investigated by several researchers. With biodiesel and blends, BSFC increases by 10–15% due to the lower calorific value of biodiesel. Engines were able to develop rated horsepower with reduced soot and particulate emissions (20–40%); however, there was an increase in NO_x emissions (4–10%). A decrease in NO_x emissions has also been reported by a few researchers. Biodiesel fuel coupled with engine architecture, operating conditions, fuel-injection system and duty cycles of the engine play an important role in the increase/decrease of emissions such as NO_x, THC, CO, etc. From the discussion given above, B5 to B10 blends of CME can be considered for

use in the locomotive engines in India considering the availability of feedstock, and effect on engine performance, emissions and durability.

The above research on utilization of CME in diesel engines has been carried out on diesel engines with displacements ranging from 0.5 to 61 DI and IDI engines, single-cylinder and multi-cylinder engines with speeds ranging from 1800 to 4800 r/min. The locomotive diesel engine used in the present study is a medium-speed (1050 r/min maximum) large-bore (11 l/cylinder) DI diesel engine. Combustion of CME in small-displacement high-speed diesel engines and its effect on the engine performance and emissions cannot be simply extrapolated onto the large-bore locomotive engines. This is because engine speed, mass flow rates of air, difference in swirl rates, difference in fuel-injection equipment and combustion chamber design play an important role in fuel-injection delays, physical and chemical delays and finally the premixed and mixing-controlled combustion. It therefore becomes imperative to experimentally evaluate the performance, emissions and combustion characteristics of CME in a large-bore locomotive engine.

Biodiesel production and characterization

Production of biodiesel was carried out by the process of esterification of free fatty acids using H_2SO_4 as a catalyst, followed by transesterification of triglycerides using sodium methoxide as a catalyst. Various physical, chemical and thermal properties of biodiesel (CME) thus prepared were evaluated (Table 2) to comply with Indian Biodiesel Standard IS 15607(2005).

CME biodiesel meets all Indian biodiesel specifications, except carbon residue, acid value and oxidation stability. The biodiesel was tested for its properties after 6 months storage in ordinary conditions, without nitrogen cover and without addition of antioxidant additives. This may be a possible reason for the lower oxidation stability and higher acid value. Possible reason for the increase in carbon residue may be contamination during transportation and storage in large fuel tanks prior to the experiment. Transesterification of the cottonseed oil is complete and is reflected by mono, di and triglyceride contents (Table 2). CME has higher density and viscosity in comparison to mineral diesel, which is in agreement with earlier studies.[1,2] Cottonseed oil is used as feedstock for biodiesel manufacturing in the present study therefore CME was tested by GC and thermo gravimetric analysis (TGA) and the results are shown in Table 3.

GC of biodiesel shows that 42% of the esters are polyunsaturated linoleic acid methyl ester (C18:2), 19% are monounsaturated oleic acid methyl ester (C18:1) and only 16% are saturated palmitic acid methyl ester (C16:0). These findings corroborate well with an earlier study of CME, which showed predominance of linoleic acid, palmitic acid and oleic acid esters.[1,9] The viscosity, cetane number, pour point and calorific value of fatty compounds increases with increasing carbon chain length and decreases with increasing unsaturation.[10] Fuel composition has a direct bearing on fuel-injection characteristics, vaporization and charge formation, therefore on the engine combustion and emissions also. Table 3 shows that a major fraction (94.1%) of biodiesel

Table 2. Important fuel characteristics of cottonseed biodiesel.

No.	Property	Test method	BIS15607 limits	CME
1	Density at 15 °C (kg/m^3)	ISO 3675, ISO 12185	860–900	887
2	Kinematic viscosity at 40 °C (cSt)	ISO 3104	2.5–6.0	5.44
3	Flash point (Pensky Marten's Closed Cup) (°C, min)	IS 1448 P:21	120	144
4	Sulfur (mg/kg, max)	ASTM D-5453	50	42
5	Carbon residue (Ramsbottom) (% w/w, max)	ASTM D-4530/ISO 10370	0.05	0.18
6	Sulfated ash (% w/w, max)	ISO 6245	0.02	0.01
7	Water / water and sediment (ppm)	ASTM D-2709, ISO 3733, ISO 6296	500	< 500
8	Cu corrosion (3 hrs at 50 °C, max)	ISO 2160	1	1
9	Cetane number (min)	IS 5156	51	56
10	Acid value (mg KOH/gm, max)	IS-1448, P:1/Sec 1	0.5	0.71
11	Methanol (% w/w, max)	EN 14110	0.2	0.095
12	Free glycerol (% w/w, max)	ASTM D-6584	0.02	0.0034
13	Total glycerol (% w/w, max)	ASTM D-6584	0.25	0.032
14	Phosphorous (mg/kg, max)	ASTM D-4951	10	< 1
15	Oxidation stability, at 110 °C (hr, min)	EN 14112	6	2.21
16	Sodium and potassium (mg/kg, max)	EN 14108 & EN 14109	To report	2 and < 1
17	Calcium and magnesium (mg/kg, max)	EN 14108 & EN 14109	To report	< 1 and < 1
18	Iodine value	NMR method	To report	98.8
19	Cold Filter Plugging Point (CFPP) (°C, max)	ASTM D 6371	Winter 6 °C Summer 18 °C	3 °C
20	Pour point (°C, max)	ASTM D 97	Winter 3 °C Summer 15 °C	0 °C
21	Monoglyceride content (% w/w, max)	ASTM D 6584	0.8 (as per EN 14105)	0.0031
22	Diglyceride content (% w/w, max)	ASTM D 6584	0.2 (as per EN 14105)	Nil
23	Triglyceride content (% w/w, max)	ASTM D 6584	0.2 (as per EN 14105)	Nil
24	Calorific value (MJ/kg)	ASTM D 240 09	–	41.415

Table 3. GC and TGA analysis of cottonseed oil and biodiesel.

Fatty acid composition by GC (% w/w)				
Formula	Name	Cottonseed oil[9]	Cottonseed oil	CME (biodiesel)
C14:0	Myristic acid	0.8	–	2.5
C16:0	Palmitic acid	24.4	23.5	29.1
C18:0	Stearic acid	2.2	7.3	5.6
C20:0	Arachidic acid	–	1.1	–
C16:1	Palmitoleic acid	0.4	–	2.2
C18:1	Oleic acid	17.2	21.3	19
C18:2	Linoleic acid	55	44.6	41.6
C18:3	Alpha linolenic acid	0.3	2.2	–
TGA analysis of CME (biodiesel)				
Weight loss		(% w/w)		
200 °C		24.9		
300 °C		94.1		
400 °C		96.6		
500 °C		99.1		

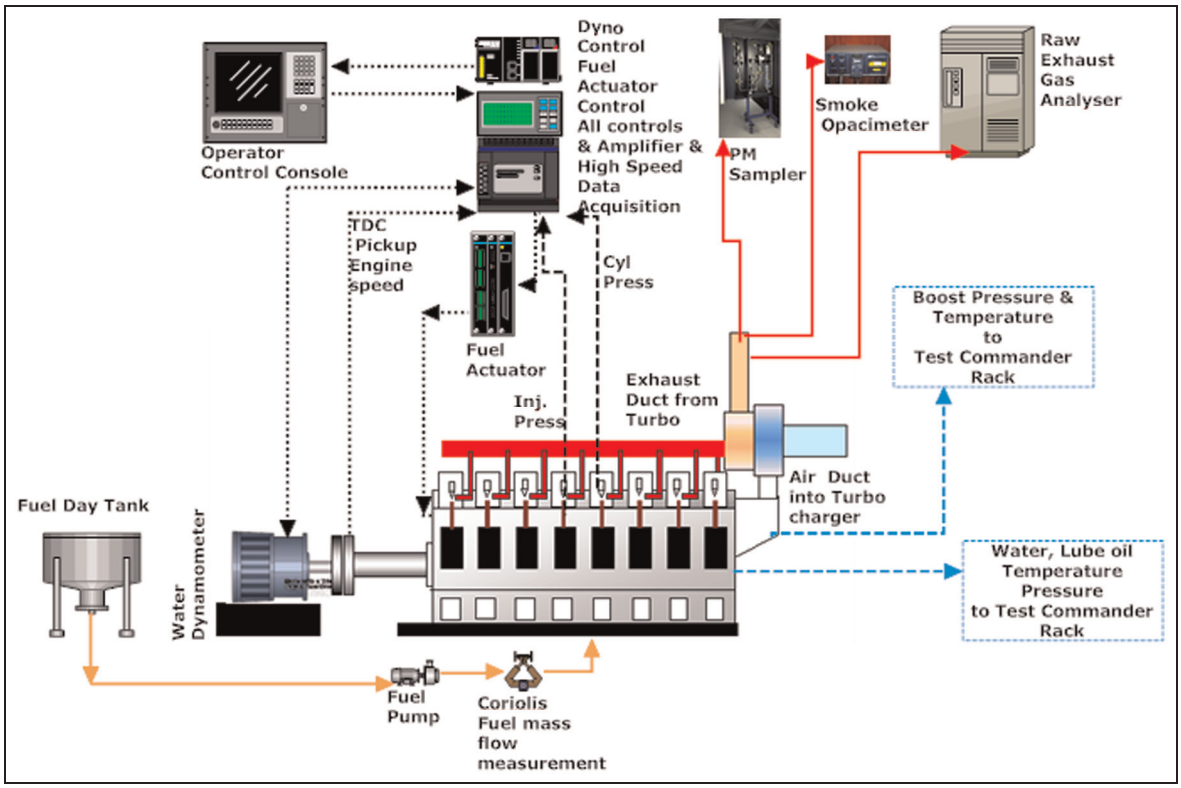

Figure 1. Schematic of the experimental setup.

evaporates below 300 °C, with the remaining fraction evaporating below 500 °C. Low-temperature heat release in hydrocarbons is generally known to occur up to 500 °C therefore the evaporation temperatures of various constituents of biodiesel become important.

Experimental setup

The schematic diagram of the experimental setup is shown in Figure 1.

The locomotive diesel engine is coupled with a hydraulic dynamometer (Zollner, Germany: 12n65f). The fuel is supplied by an electronically controlled fuel actuator (FVG: 9400). Fuel flow rate is measured by a Coriolis fuel flow meter (Emerson: Micromotion CSM 50). Both the dynamometer and fuel actuator are controlled by an engine test control unit (AVL, Austria: PUMA Open). The locomotive engine operates on nine preset speed and torque points called 'notches', numbered from zero to eight. Engine speed, temperatures and pressures of intake air, exhaust, water, lubricating oil, etc. are recorded by the test control unit. In-cylinder pressure was measured by a water-cooled piezoelectric pressure transducer (AVL, Austria: QC34C). A charge

Table 4. Specifications of the exhaust gas emission analyzer (AVL, Austria: AMA4000) and Smoke Opacimeter (AVL, Austria: 435).

Pollutant	Measurement principle	Range	Least count	Repeatability
NO_x	Chemiluminiscence	0–10,000 ppm (4 ranges)	10 ppb	$\leqslant$0.5% of FS
THC	Flame ionization detection	0–2000 ppm C_3 (4 ranges)	30 ppb THC	$\pm$0.5% FS
CO_2	Non-dispersive infrared (NDIR)	0–20%	$\leqslant$0.3 % of lowest range, 600 ppm CO_2	$\leqslant$0.5% FS
CO	NDIR	50–5000 ppm	$\leqslant$0.3 % of lowest range, 150 ppb CO	$\leqslant$0.5% FS
Smoke opacity	Light extinction	0–100%	0.1% of full scale (FS)	0.1% for 30 minutes

amplifier (AVL, Austria: 3066) is used to generate an output voltage proportional to the charge generated by the piezoelectric pressure transducer. A precision shaft encoder (AVL, Austria: 365x) with a crank angle (CA) resolution of 0.5 crank angle degrees (CAD) is used for determining the crankshaft position. The high-pressure fuel line and fuel injectors were instrumented to find the fuel-line pressure and the injector needle lift respectively. A Hall-effect proximity sensor was used to measure the needle lift in the fuel injector. In-cylinder pressure–CA history, fuel-injection pressures, injector needle lift with respect to shaft encoder signals are recorded by the high-speed data acquisition system (AVL, Austria: Indimaster). Emissions are measured by raw exhaust gas emission analyzers integrated into an AVL emissions test bench (AVL, Austria: AMA4000). For emission measurements, exhaust gas temperatures were maintained at 190 °C using a heated exhaust sampling line. NO_x and HC emissions were measured without cooling the exhaust. All gaseous emissions were measured continuously during testing, and measurements were automatically recorded by the data acquisition system every 15 s via serial communication ports. Table 4 shows the measurement principle, accuracy and repeatability of raw exhaust gas emission analyzers/measuring equipment for various exhaust gas species.

Particulate matter (PM) is collected on a pre-conditioned filter paper using a partial flow dilution tunnel sampler (AVL, Austria: SPC 472). Smoke opacity is measured using a smoke opacimeter (AVL, Austria: 435). Rate of heat release was calculated from the in-cylinder pressure–CA data collected for a large number of consecutive engine cycles and averaged thereafter for further analysis.

Test points

For thermal stabilization, the engine was first notched up in pre-determined time steps from idle to the eighth engine notch. The engine coolant temperature was then allowed to stabilize and the measurements were taken starting with the eighth engine notch downwards. Three biodiesel blends (B10, B20, B50) and biodiesel (B100) were experimented with vis-a-vis baseline data from mineral diesel. Because of the special operating conditions for locomotives, United States Environmental Protection Agency (USEPA) has worked out a separate test cycle for evaluation of diesel locomotive engines.

All research reported on locomotive engines has evaluated the engine at pre-determined notches.[12–17] Accordingly, engine performance, emissions and combustion measurements in the present research is also carried out on these nine pre-determined engine notches. The experiments were performed three times for each engine operating point and the average reading was used for further data analysis.

Results and discussion

Engine load lines for the locomotive engine are shown in Figure 2. The maximum power generated by the locomotive engine is 2312 kW at 1050 r/min for the eighth notch, which corresponds to 15 bar brake mean effective pressure (BMEP). The maximum torque generated by locomotive engine is approximately 22,000 Nm (Figure 2).

Figure 3 shows the power developed by the engine with diesel, biodiesel and various blends of biodiesel. With B100, the engine was able to develop rated power identical to mineral diesel. This is an indication of sufficiently large fuel delivery capacity of the fuel-injection equipment. The BSFC of CME fueled locomotive engine is higher than the mineral diesel and brake thermal efficiency (BTE) for biodiesel blends is relatively lower compared to mineral diesel (Figure 3). The difference in BSFC is higher at lower engine notches, e.g. at the idling notch, it is 15.4% and at the eighth notch, it is 12%. No change in BTE is observed up to B20 at all engine notches however this reduces for B50 and biodiesel. The reduction in BTE is less pronounced at higher notches (1% for B100 at eighth notch) than at lower notches (2% for B100 at idle notch). For the mechanical pump–line–nozzle (PLN) system used in the locomotives, optimization of the start of fuel injection is carried out for the eighth notch. This difference in BSFC and BTE at different notches for various test fuels is possibly due to sub-optimized engine operation at other operating points.

Figure 4 shows the relationship of BSFC of the test fuels with the lower heating value (LHV) of the fuels and with BTE at different engine operating points. The BSFC increases for biodiesel and blends due to lower LHV of biodiesel and also due to lower fuel conversion efficiency (BTE) obtained from these oxygenated fuels. The BSFC differences between these test fuels are largely due to different LHV while minor impact is due to differences in BTE (Figure 3). Figure 5 shows the

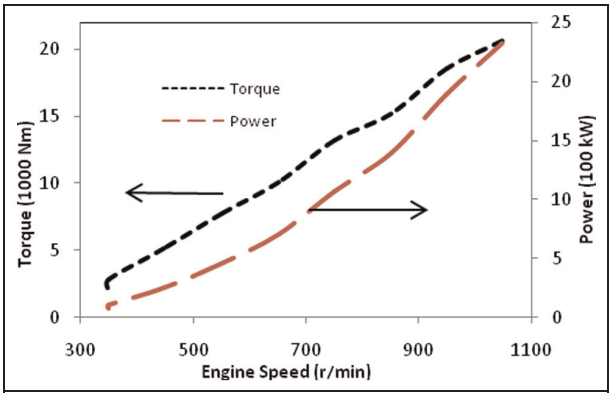

Figure 2. Locomotive engine load lines.

combustion efficiency for different test fuels at different notches. The combustion efficiency shows an increasing trend with increasing fuel oxygen, confirming earlier findings.[18] Higher fuel-injection pressure, longer flame lift-off length, larger O/C ratio at the flame lift-off length, and higher low-temperature heat release (LTHR) with biodiesel may be some of the possible reasons for higher combustion efficiency with biodiesel.[19–21] Biodiesel also contains unsaturated HCs (double bonds) and molecular oxygen (Table 3), which influences combustion and thereby in-cylinder temperatures.[10]

Figure 6 shows the dependence of combustion efficiency on the emissions of THC, CO and PM. Heywood[22] suggested that the energy lost in the

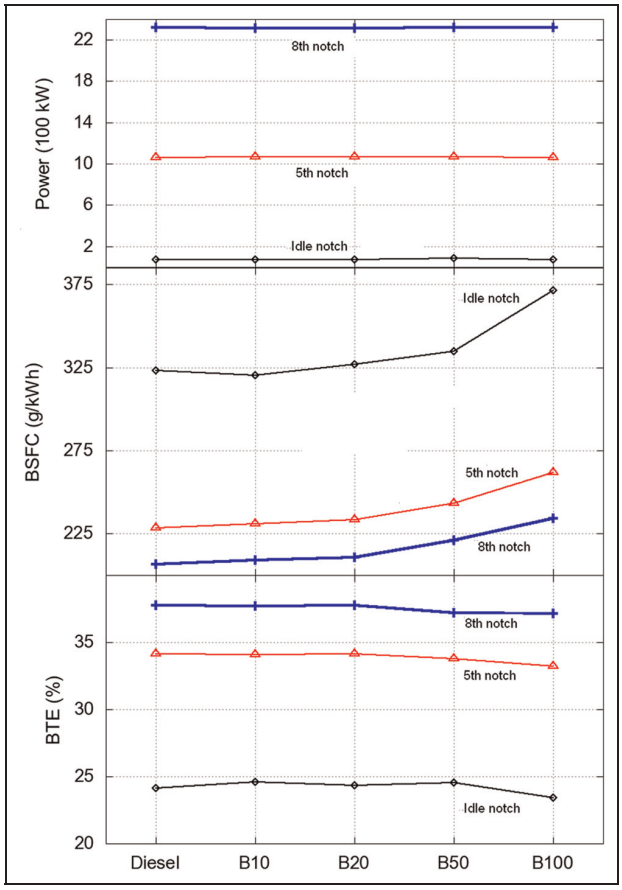

Figure 3. Power, BSFC and BTE of locomotive engine.

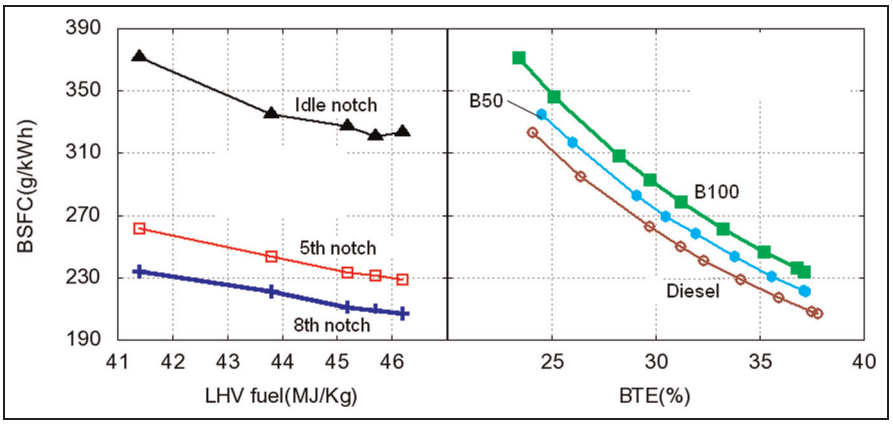

Figure 4. Dependence of BSFC on the calorific value of fuel and brake thermal efficiency.

exhaust in the form of the emissions of THC, CO and PM determines the combustion inefficiency of the engine. Figure 6 illustrates that for the engine under investigation, the relationship between the combustion efficiency and emissions of CO and PM shows the trend enumerated by Heywood. In the case of HC emissions, initially a reverse relationship exists between the combustion efficiency and the THC emissions. This relationship does not hold for higher HC emissions however. This is due to the effect of CO and PM emissions becoming dominant, and the energy loss due to HC emissions becoming relatively less dominant.

For this engine, boost pressure builds up from the fifth notch onwards. At lower notches, the engine operates practically naturally aspirated. Pre-turbine exhaust gas pressures increase with increasing notches. Up to sixth notch, diesel and biodiesel result in highest pre-turbine exhaust pressures; however, for the seventh and eighth notches, B10 and B20 show highest pre-turbine exhaust pressures (Figure 7). Miyamoto et al.[18] showed

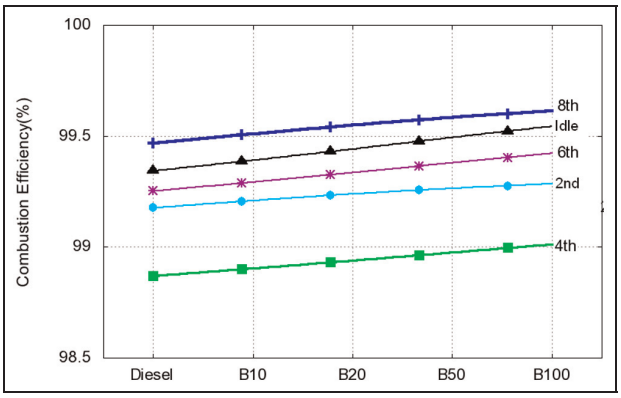

Figure 5. Combustion efficiency for various test fuels.

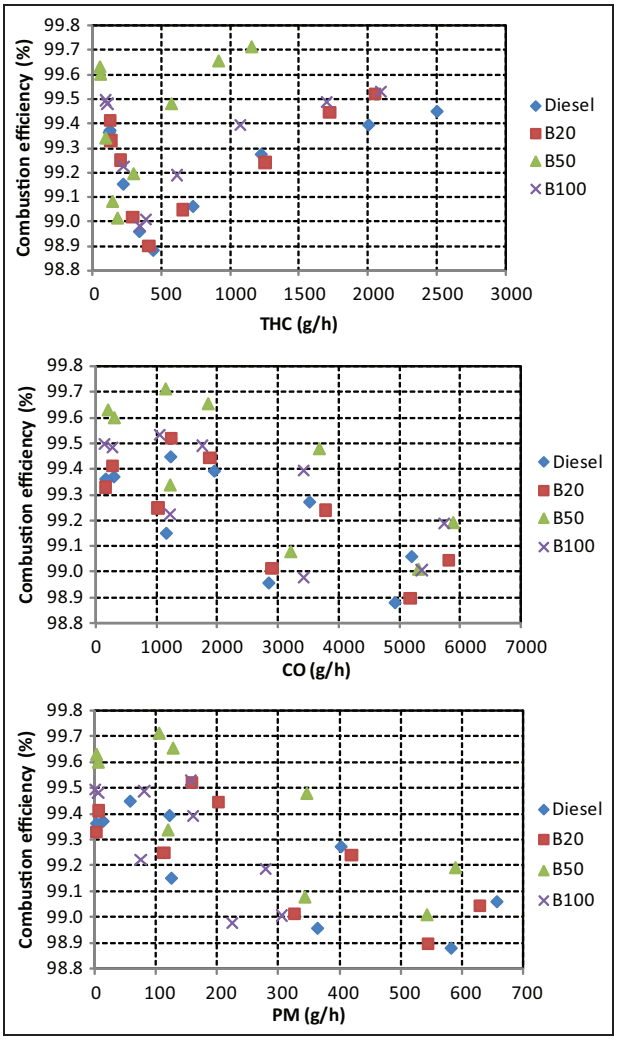

Figure 6. Combustion efficiency as a function of THC, CO and PM.

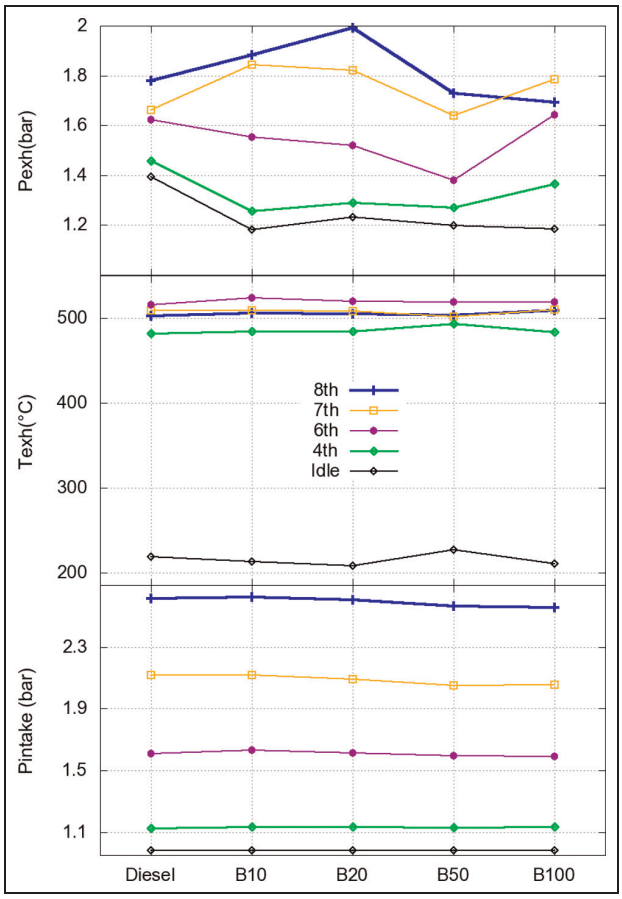

Figure 7. Exhaust gas pressure, temperature and inlet manifold air pressure for various test fuels.

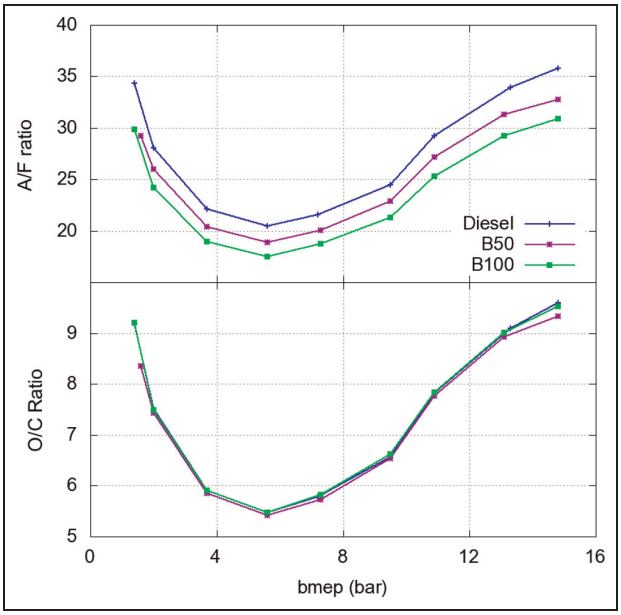

Figure 8. A/F and O/C ratios for various test fuels.

increase in the number of molecules in the exhaust with oxygenated fuel in a compression-ignition (CI) engine. Difference in the number of molecules in the exhaust may be a possible reason for the difference in the exhaust pressures for different fuels. Very high exhaust gas temperatures are obtained at the fifth, sixth, seventh and eighth notches, in that order, due to low O/C ratios at intermediate notches (Figure 8). The O/C (w/w) ratio here refers to the total oxygen (air and fuel) (w/w) in the combustible mixture to total carbon in the fuel. For biodiesel, carbon and oxygen content in the fuel is

obtained from GC analysis. Oxygen originates from air and fuel (biodiesel) both. For diesel, the standard formula given in the published literature[22] has been used to calculate the O/C ratio.

The air-to-fuel (A/F) ratio decreases as the percentage of biodiesel in the blend increases (Figure 8). This is a consequence of the lower calorific value of biodiesel and its blends. The O/C ratio, however, remains nearly constant for all test fuels (Figure 8). Fuel oxygen compensates for the lower A/F ratio for biodiesel and blends. The fourth and fifth notches have lower A/F and O/C ratios and are relatively closer to the stoichiometric O/C ratio, a factor responsible for the highest average exhaust gas temperatures. Although lower notches (third to fifth) have lower O/C ratios, relatively lower exhaust gas temperatures are obtained due to the lower fuel quantity injected. Inlet manifold air pressure remains nearly constant for all test fuels, albeit a slight dip is observed at higher notches for B50 and biodiesel. Inlet manifold air pressure (compressor outlet pressure) is affected by the total enthalpy of the exhaust gas (at the turbine inlet).

Start of injection (SOI) is taken as the CA at which the fuel injector needle lifts 0.01 mm. The SOI of biodiesel is seen to have advanced compared to mineral diesel throughout the entire load and speed range. This corresponds to lower injection delay for biodiesel and blends compared to mineral diesel (Figure 9). A decreasing trend in SOI timing with increasing bulk modulus for different fuels at three representative engine notches is observed (Figure 9). At higher engine notches, an advance in SOI with increasing bulk modulus is prominently observed. The locomotive engine under investigation employs a PLN system. SOI has a significant effect on the BSFC, NO_x, PM and THC emissions; therefore, injection delay becomes a key parameter.

Injection delay has been calculated based on empirical and theoretical relationships and compared with the experimental results (appendix 1). Injection delay in a PLN system is likely to depend on the following factors.

1. Speed of sound in the fuel: depending on the length of the high-pressure pipe, the time taken by the pressure wave to travel to the injector needle will be higher or lower.
2. Compressibility of the fuel's bulk modulus of compressibility: a higher compressibility will result in higher compression pressures for the same amount of compression and earlier injector needle opening.
3. Viscosity of the fuel: a higher viscosity of the fuel should reduce the leakage of the fuel past the fuel-injection pump plunger and aid in faster buildup of pressure in the fuel injection system.

Total advance in start of fuel injection due to differences in the speed of sound and bulk modulus is found to be 0.4 CAD. This is less than the measured value of 0.93 CAD. This difference may be due to the inaccuracies in the estimation of the injection system parameters

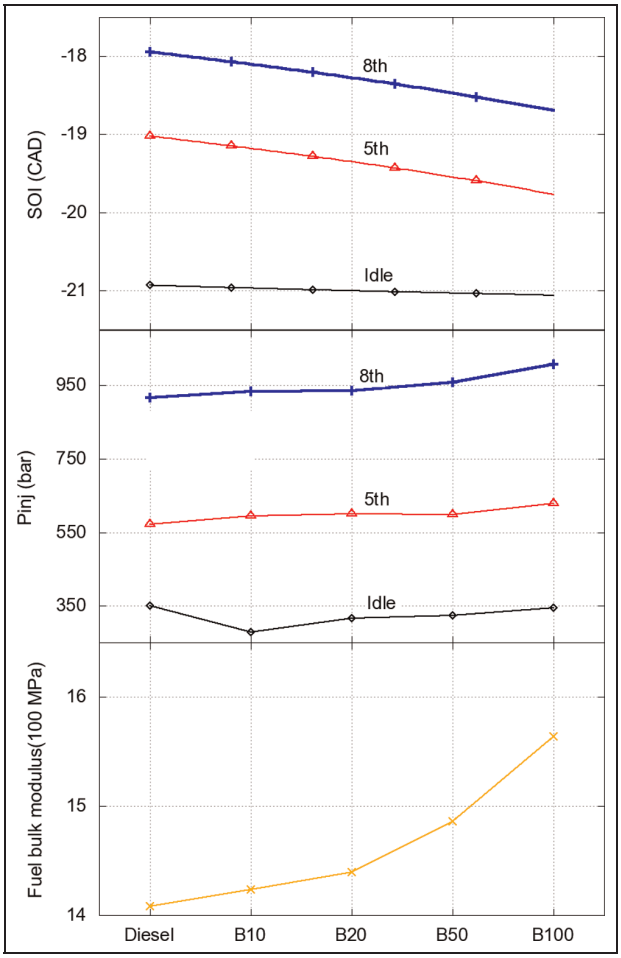

Figure 9. Start of injection, injection pressure and bulk modulus of various test fuel.

and also due to the additional effect of viscosity, which is not accounted for in the calculations. A regression analysis was carried out to establish dependency of SOI on the bulk modulus of the fuel. The regression analysis shows that at the eighth and fifth notches, a statistically significant correlation exists between the SOI and the bulk modulus of the fuel with R^2 values of 0.91. However at the idle notch, this correlation is found to be weak.

Exhaust emissions

Emission characteristics of the locomotive engine were evaluated for mineral diesel, biodiesel and their blends. Regulated emissions such as NO_x, THC, CO, CO_2, PM and smoke opacity (Figure 10) were investigated in this study. Emissions are reported in terms of percentage of the maximum value obtained vis-a-vis mineral diesel (in order to protect business interests). For this, first the raw emissions are converted to mass emissions (g/kWh) and then converted to percentages compared to mineral diesel for various test fuels.

The engine produces highest brake specific NO_x ($BSNO_x$) emissions for B100 among all test fuels at all notches and in conformity with earlier findings as

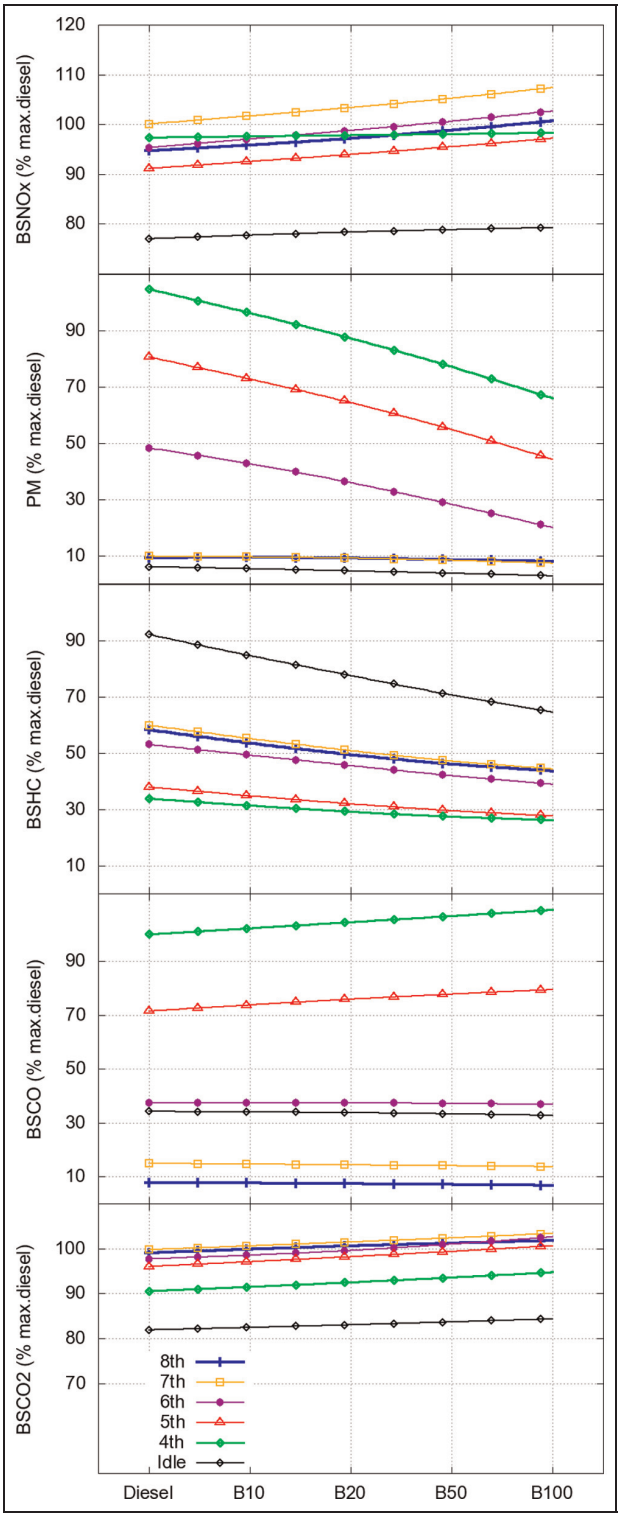

Figure 10. Brake-specific mass emissions of exhaust species for various test fuels.

explained further. At fourth notch, $BSNO_x$ emissions remain constant, irrespective of the fuel used. This is in agreement with earlier findings that NO_x emission is a function of engine operating conditions in addition to factors like fuel, engine architecture, etc.[23] Lowest $BSNO_x$ emissions are measured from diesel at the idle notch (70% of maximum obtained with diesel), whereas the highest $BSNO_x$ emissions are obtained with biodiesel at the seventh notch (108% of maximum obtained with diesel). Mineral diesel showed lowest $BSNO_x$ emissions at higher engine loads (80–90% of the rated). At the fourth notch, the NO_x emissions are not sensitive to the fuel. This may be due to combination of temperature and oxygen at this engine operating point, since NO_x emissions are dependent both on the temperature and on the oxygen concentration of the fuel/air mixture. Increase in $BSNO_x$ emissions from diesel engines using biodiesel has been reported by many researchers. Mazumdar and Agarwal[24] observed that NO_x increased with increased concentration of biodiesel in the blends. Nabi et al.,[2] Rakopoulos et al.[3] and Savvidis et al.[7] also reported increase in NO_x emissions up on use of CME in different displacement CI engines. Capareda et al.,[6] however, reported reduction of 14% NO_x emissions from CME in a 14.2 kW engine. Kousoulidou et al.[25] performed experiments using B10 (palm oil) and rapeseed methyl ester (RME) on a light-duty common-rail Euro III engine and observed only marginal effects on NO_x over the baseline diesel emissions.

The PM emissions decrease with increasing percentage of biodiesel in the blends. PM emissions are found to be highest for mineral diesel and 70% (of maximum) with B100 at the fourth notch. The effect of oxygenated fuels like CME in reducing PM is predominant at intermediate notches (fourth, fifth and sixth). At higher and lower notches, PM emissions from the engine are already quite low, hence PM emission does not decrease any further upon use of CME and blends. Reduction in PM with use of CME blends has also been reported in earlier studies.[2,3,7,8] NO_x and PM formation mechanism using CME compared to mineral diesel are discussed in detail later in this paper.

The biodiesel fueled engine emits the lowest brake specific hydrocarbons (BSHCs) at all notches, producing 30–70% BSHC compared to diesel fueled locomotive engine. Song and Zhang[26] studied the effect of soybean oil methyl ester and blends (B10, B20, B30, B50, B80 and B100) and found reduced HC emissions with increase in biodiesel content in the test blends at partial engine loads. At full load, HC emissions from biodiesel engine were closer to diesel engine because HC emissions from diesel were already very low at full load. In the present experiment, highest BSHC emissions were measured at idle notch and the lowest at fourth notch (Figure 10). BSHC emissions at higher notches were somewhere in between. HC formation is a result of partial combustion of fuel, and presence of fuel oxygen in biodiesel aids combustion, thereby reducing HC emissions. Another possible reason may be earlier fuel injection with biodiesel (as seen in Figure 9), hence, more time availability for mixing, combustion and oxidation. Relatively lower volatility of biodiesel may however hamper the formation of combustible mixture at the fringes of the spray.[26]

Brake specific carbon monoxide (BSCO) and brake specific carbon dioxide ($BSCO_2$) emissions are highest,

when the engine is fueled with B100, and are lowest with mineral diesel. Higher emissions of BSCO and $BSCO_2$ with B100 are reportedly due to carboxylation of the ester molecules in biodiesel.[27] BSCO emissions increase with increase in biodiesel content in the test fuels at third, fourth and fifth notches. For other notches, biodiesel does not have any significant effect on BSCO emissions. The O/C ratio of the air–fuel mixture is lowest at the third, fourth and fifth notches (Figure 8), resulting in higher CO emissions. At other engine notches, higher O/C ratios suppress formation of CO. Increase in the $BSCO_2$ emissions in biodiesel fueled engine is due to early carboxylation of ester moiety and relatively more complete combustion of the air–fuel mixture. $BSCO_2$ increases as the biodiesel content in the test fuel increases. Szybist et al.[28] found that CO_2 production occurs in the early stages of combustion due to decomposition of fuel, whereas this phenomenon could not be seen in a diesel surrogate fuel 'n-heptane'. Thus, CO_2 production in biodiesel fueled engines follows additional pathways other than oxidation of carbon.

Factors affecting NO_x emissions from the biodiesel fueled CI engine are (a) SOI, (b) global air–fuel equivalence ratio, (c) temperature of the inlet air, (d) timing and magnitude of maximum in-cylinder temperatures, (e) ignition delay, and (e) structure of the biodiesel molecule, unsaturation level/iodine number, etc.[6,7,25,29] The NO_x emissions are predominantly affected by the timing of the start of combustion process, which in turn is governed by SOI, the timing of maximum in-cylinder gas temperature and the timing of maximum heat-release rate. The dependence of $BSNO_x$ emissions on these factors is shown for diesel, biodiesel and blends in Figure 11. Each point for a notch represents one test fuel: diesel, biodiesel and blends.

NO_x formation is a kinetically controlled process and begins well after the SOC in the high-temperature zones of the post-flame region. Equilibrium for NO_x emissions at lower temperatures is not achieved as the concentration becomes kinetically frozen during the expansion stroke. Therefore, earlier is the start of formation of NO_x, the higher will be its concentration and vice-versa. Figure 11 confirms these findings. NO_x emissions are found to be proportional to the start of injection timings. Similarly, the timings of maximum in-cylinder temperature and the peak heat-release rate determine the final NO_x concentration in the exhaust. Similar findings have been reported in earlier studies by Szybist et al.[30] In the present study, $BSNO_x$ emissions are not strongly related to maximum mean cylinder temperature and ignition delay (Figure 11). Correlation of the NO_x emissions to the structure of the biodiesel molecules and unsaturation level/iodine number is beyond the scope of the present study.

Vioculescu and Borman[31] measured cylinder-averaged NO_x emissions in a diesel engine and found

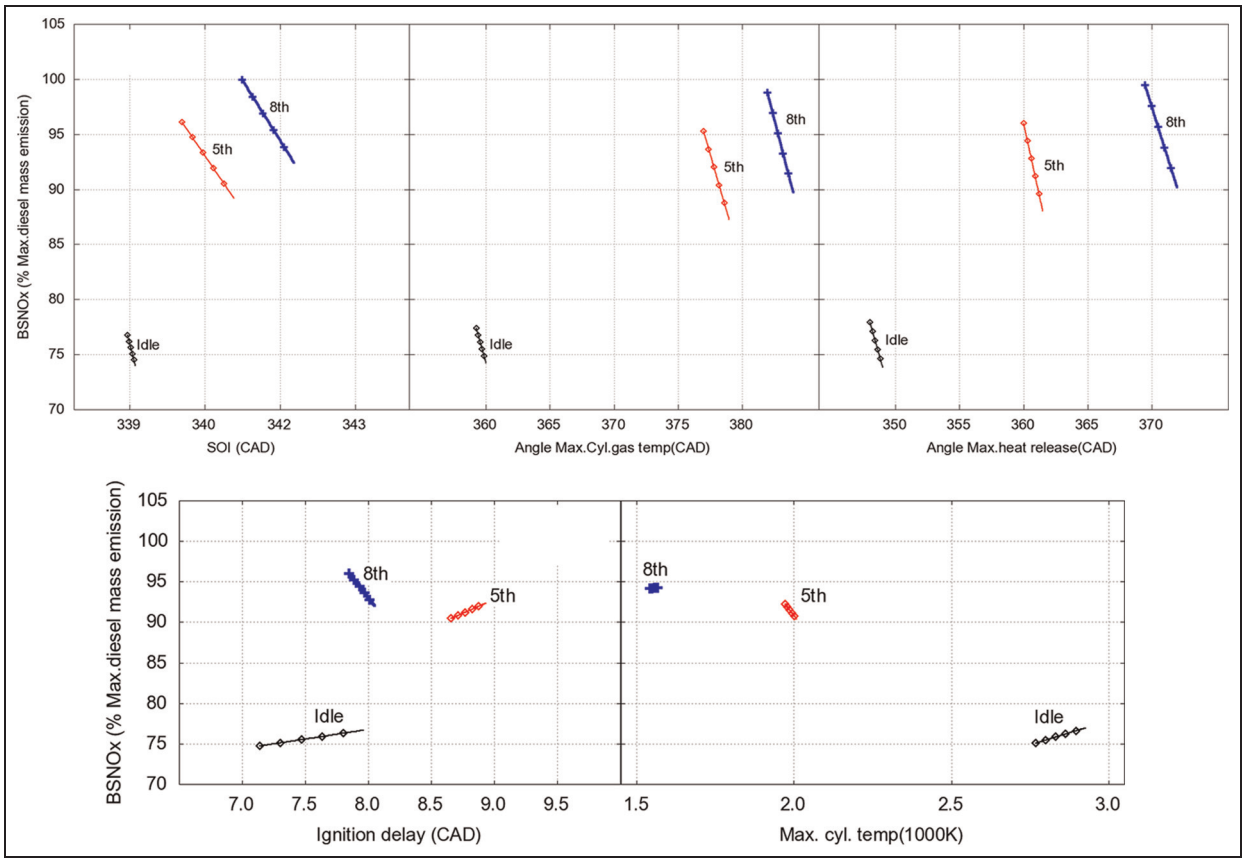

Figure 11. Effect of fuel-injection timing, timing of maximum mean gas temperature, timing of maximum heat release, ignition delay, and maximum mean gas temperature on $BSNO_x$.

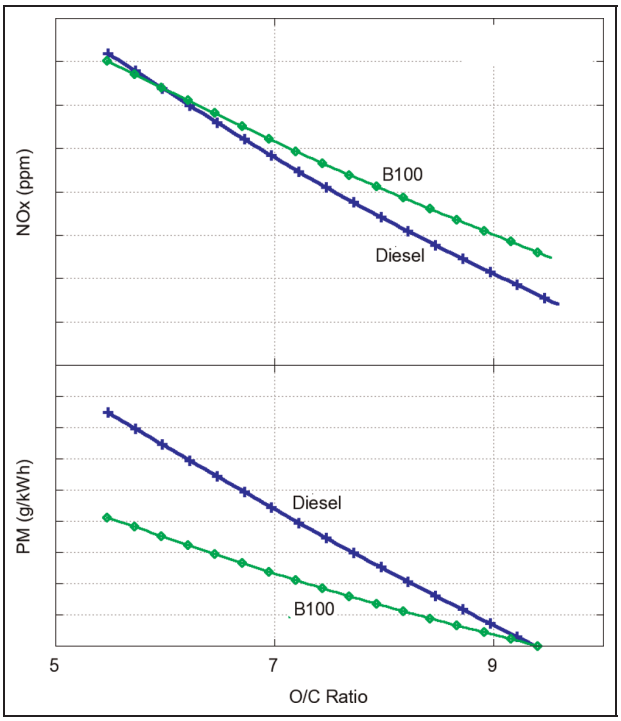

Figure 12. PM and NO_x emissions for varying O/C ratios.

that the NO_x emissions increase as the overall equivalence ratio (ϕ) became closer to stoichiometric. In the present study, O/C ratio is considered to be a better index compared to ϕ because of the use of oxygenated fuels. For a stoichiometric mixture, the O/C ratio (w/w) is 3.88 for mineral diesel. Since there is no oxygen present in mineral diesel, this ratio would depend only on ϕ; however, for an oxygenated fuel such as biodiesel or blends, this would also depend on the oxygen content of the test fuel. Figure 12 shows raw emission of NO_x (ppm) and PM (g/kWh) against O/C ratio for B100 and diesel, in order to have a direct comparison. O/C ratio has been calculated for all notches for biodiesel and diesel.

A phenomenon similar to the one reported by Vioculescu and Borman[31] has also been observed in the present study. For the same O/C ratio, B100 emits relatively higher NO_x and lower particulates compared to mineral diesel. Below O/C ratio of 6, there is no appreciable difference in NO_x emissions from diesel and biodiesel. As the O/C ratio moves towards the stoichiometric value of 3.88, NO_x emissions are expected to increase as reported in the earlier findings of Vioculescu and Borman.[31] A similar trend is also observed for PM. The equilibrium reaction predicts that soot formation in the flames should occur when the atomic C/O ratio exceeds unity ($m > 2y$) (equation (1)),[22] or the mass O/C ratio is less than 1.33

$$C_mH_n + yO_2 \rightarrow 2_yCO + n/2H_2 + (m - 2y)C_s \qquad (1)$$

In the present study, as the O/C ratio decreases, the PM emissions increase. Note that with biodiesel, the increase in PM emission with reduction in O/C ratio is relatively lower than diesel. Earlier studies have suggested following reasons for relatively lower smoke opacity and PM emission with biodiesel and blends: (a) presence of fuel oxygen, (b) increase in the O/C ratio at the flame lift-off length, (c) longer flame lift-off length due to higher injection velocity obtained with biodiesel, and (d) superior fuel atomization due to higher injection pressures with biodiesel.[32,33] Graboski and McCormick[34] reported a reduction in PM emissions with an increase in oxygen (w/w) in biodiesel blends. Similarly, Flynn et al.[33] demonstrated that as fuel oxygen (w/w) increases, there is a significant reduction in the percentage of fuel carbon, which forms soot precursors. They found that the predicted level of soot the precursors correlates well with the soot emissions from a diesel engine. Siebers[35] suggested that soot production in an engine decreases as the O/C ratio in the liquid fuel at the flame lift-off length increases. Siebers and Higgins[32] measured flame lift-off lengths for a diesel flame at different pressure drops across the injector orifice for a range of injector orifice diameters, and concluded that the flame lift-off length increases as the pressure drop across the injector orifice increases. In the present study, an injector with an orifice diameter of 0.38 mm has been used. Siebers and Higgins[32] used several orifice diameters for their research, and the closest orifice diameter to the present research was 0.363 mm. Therefore, measurements made with 0.363 mm diameter injector orifice have been used to calculate the difference in the flame lift-off lengths in the present study (with diesel and CME). It is assumed that the flame lift-off length of biodiesel blends will be within these outer limits. Maximum fuel injection pressure at the eighth notch has been used for the flame lift-off length calculations.

Fuel-injection velocities were calculated and compared for the eighth notch for diesel and B100 (Figure 13). Fuel-injection velocities are higher throughout the injection event for B100, mainly because of higher injection pressures with B100

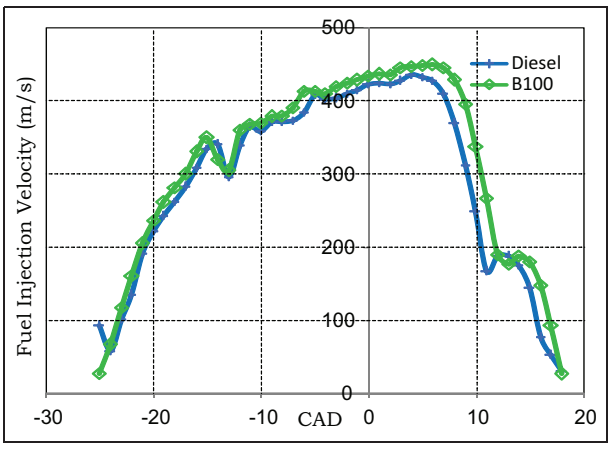

Figure 13. Fuel-injection velocities at the eighth notch for the locomotive engine.

Table 5. Summary of change in emissions, BSFC and BTE with biodiesel.

	$BSNO_x$ (norm %)		PM (norm %)		BSFC (g/kWh)		BTE (%)	
Notch	Diesel	B100	Diesel	B100	Diesel	B100	Diesel	B100
8	95	102	10	9	206.4	234.0	37.8	37.1
7	100	108	10	9	207.7	236.2	37.5	36.8
6	95	104	50	20	217.1	246.8	35.9	35.2
5	92	97	80	45	228.4	261.7	34.1	33.2
4	98	98	100	68	240.9	278.8	32.3	31.2
3	98	93	100	70	249.9	292.8	31.2	29.7
2	85	80	68	45	262.7	308.1	29.7	28.2
1	80	76	8	8	294.9	346.2	26.4	25.1
Idle	76	80	8	8	323.2	371.3	24.1	23.4

(already discussed in Figure 9). Higher fuel-injection velocities increase the lift-off length of fuel sprays in a diesel engine as reported by Siebers.[32,33,35] This in turn affects the amount of oxygen entrained in the diesel flame jet up to the flame lift-off length and determines the formation of soot precursors. This is another effect, which might possibly be responsible for reduction in smoke opacity for biodiesel.[35] Higher fuel-injection pressures will reduce the rich zone fuel-air ratio prevailing in the core of the spray, which leads to lower soot formation. This may increase the surface area of the 'stoichiometric diffusion flame sheet', which in turn increases NO_x formation and emission.[36]

A biodiesel flame with a fuel-injection pressure of 1000 bar (Figure 9) and a fuel-injection velocity of 460 m/s (Figure 13) is calculated to have a 40 mm flame lift-off length, whereas a diesel flame with a fuel-injection pressure of 900 bar and a fuel-injection velocity of 420 m/s is calculated to have a 35 mm flame lift-off length. Siebers and Higgins[33] showed that air entrainment up to the lift-off length location (as a percentage of the total air required to burn the injected fuel) is linearly dependent on flame lift-off length. They suggested that relative total soot incandescence in the flame decreases as the lift-off length/air entrainment at the lift-off location increases. Therefore, a biodiesel flame with a longer lift-off length is expected to produce less soot/PM compared to diesel. Table 5 shows a summary of brake-specific emissions with biodiesel compared to diesel at different notches.

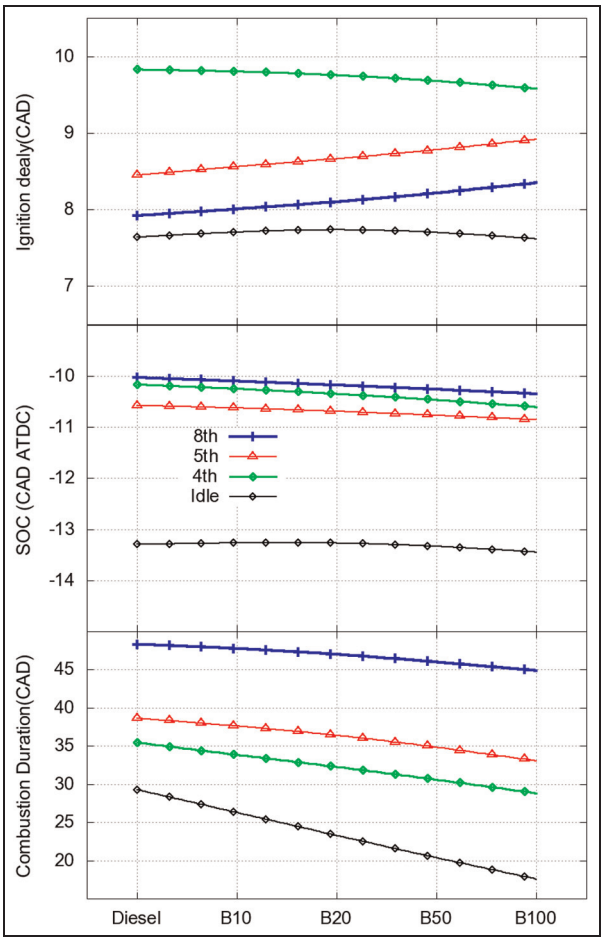

Figure 14. Ignition delay, start of combustion and combustion duration for various test fuels.

Combustion characteristics

Figure 14 presents the ignition delay (ID), SOC and combustion duration for the test fuels in the locomotive engine at different notches.

Due to fuel vaporization, heat release will adopt a negative value before SOC. SOC is the CAD at which the heat release (dQ) becomes positive again. The ID is calculated as the difference (in CAD) between SOI and SOC. With biodiesel and blends, SOC is earlier and combustion duration is significantly lower than diesel. A higher ID for biodiesel at intermediate engine notches is compensated for by earlier SOI compared to mineral diesel (Figure 9). Sinha and Agarwal[37] investigated the combustion characteristics of a rice-bran oil methyl ester fueled DI transportation diesel engine for varying loads at two speeds, and showed an earlier SOC for biodiesel at all operating points. However, they reported a higher combustion duration for biodiesel blends. This difference in findings indicates that the combustion characteristics of biodiesel and blends may be dependent on the engine architecture and size.

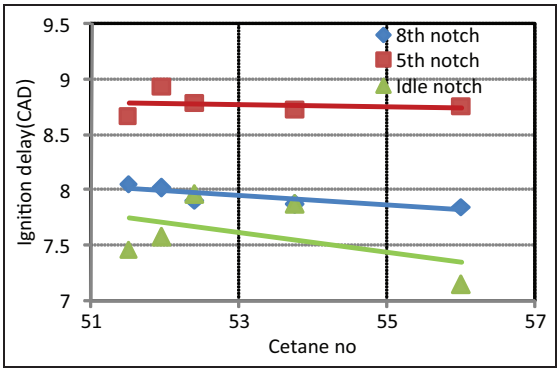

Figure 15. Ignition delay versus cetane number for various test fuels.

Table 6. Start of pressure rise for diesel and biodiesel.

	Eighth notch	Fifth notch	Idle notch
Diesel	−9 ATDC	−8 ATDC	−12 ATDC
Biodiesel	−11 ATDC	−10 ATDC	−13 ATDC

ATDC: After Top Dead Center.

other fuel properties might be responsible for a higher premixed-burn fraction, in spite of biodiesel's higher cetane numbers.[38] Measured ID as a function of cetane number of diesel, biodiesel and blends (Figure 15) does not indicate a strong and direct correlation.

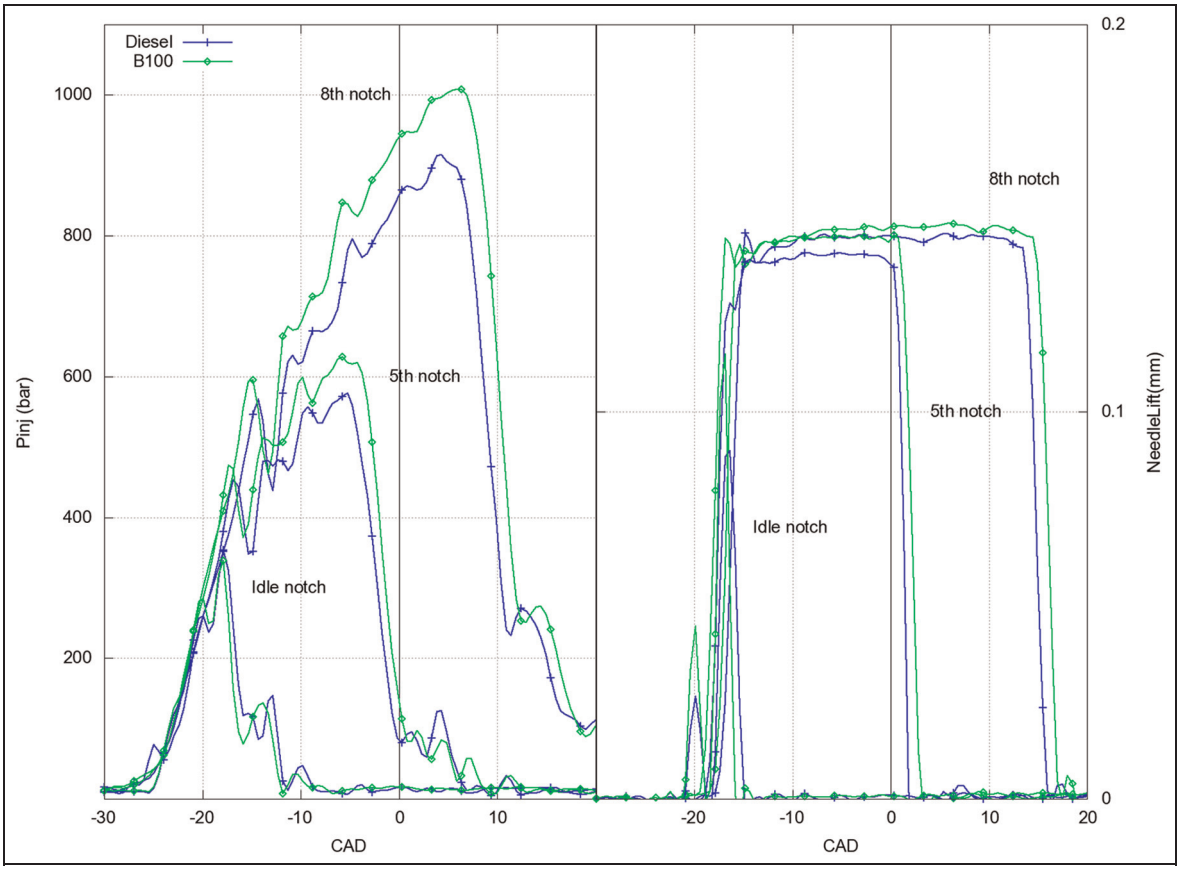

Figure 16. Fuel-line pressure and needle lift at different notches.

All test fuels show a similar trend for ID, i.e. high ID at intermediate notches (Figure 14). This is due to lower A/F and O/C ratios at the intermediate notches (Figure 8). In this case, the oxygen in biodiesel is unable to compensate for lower air availability, and relatively lower volatility of biodiesel is responsible for slightly higher ID at intermediate notches.

At a particular load, the main factor controlling the premixed combustion is ID. Shorter ID produces smaller premixed combustion. Since the cetane number of biodiesel is higher than mineral diesel, it is expected to have a shorter ID. However, the cetane number may not be an effective measure of ID for biodiesel, and

In order to find the correlation between fuel-injection timing, heat release and emissions, fuel-line pressure and injector needle lift were measured and analyzed at three notches (Figure 16).

At all three notches, fuel-injection pressure starts increasing earlier/faster for biodiesel; maximum injection pressures are higher for biodiesel; and the fuel-injection pulse is longer for biodiesel. Peak in-cylinder pressure at the eighth notch is higher than 100 bars, whereas fuel injection pressure is approximately 900 bars for diesel and 1000 bars for biodiesel. The pressure difference across the injector nozzle orifice enables liquid fuel jets to enter the combustion chamber at sufficiently high

velocity in order to (a) atomize fuel into small droplets, enabling rapid evaporation, and (b) traverse the combustion chamber in the time available in order to fully utilize the air.[27] If the pressure drop across the nozzle and nozzle open area are constant during the injection period, the mass of fuel injected is given by[22]

$$m_f = C_D A_n \sqrt{2\rho_f \Delta p}(\Delta\theta/360N) \quad (2)$$

Here, C_d is the discharge coefficient, A_n is the nozzle minimum area, and ρ_f is the fuel density. $\Delta\theta$ is the nozzle open period (CAD), N is the engine speed (r/min) and Δp is the pressure difference across the nozzle orifice. From this equation, it can be noted that as Δp increases, the quantity of fuel injected also increases, and the case with increasing $\Delta\theta$ is similar. At the eighth notch, Δp for biodiesel is approximately 900 bars, and for mineral diesel, it is approximately 800 bars. $\Delta\theta$ for biodiesel is approximately 3 CAD higher than mineral diesel (Figure 16). Injection pressures are higher for biodiesel and injection starts earlier and for a longer duration compared to diesel. The injector needle closes relatively later for biodiesel because a higher fuel quantity has to be injected into the cylinder in every cycle in order to maintain a similar power output, as shown by equation (3)[22]

$$P = (\eta_f m_a N Q_H V(F/A))/n_R \quad (3)$$

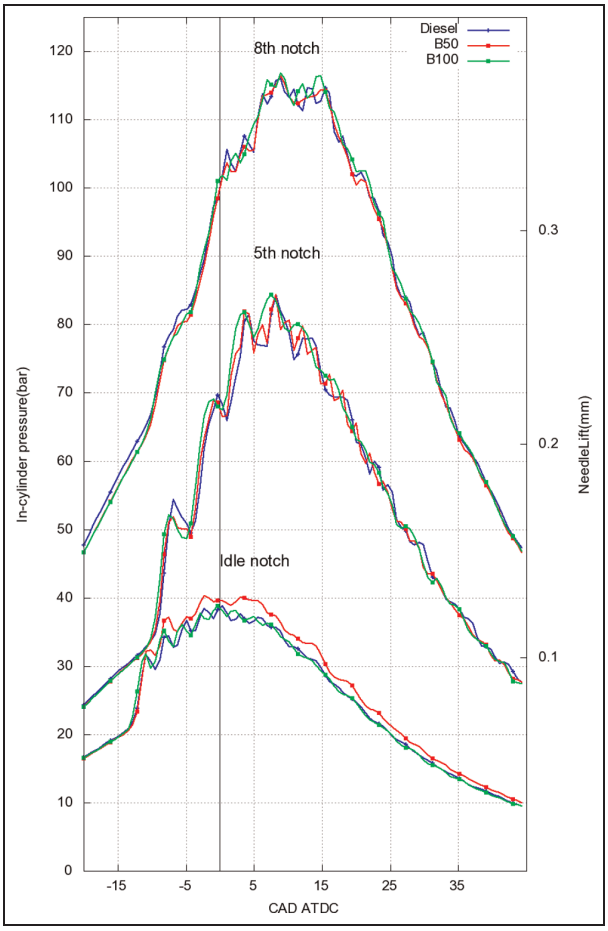

Figure 17. In-cylinder pressure–CAD for various test fuels.

where η_f is the combustion efficiency, m_a is the mass of air per cycle, N is the engine speed, F/A is the fuel–air ratio, Q_{HV} is the heating value of the test fuel and n_R is 2(for 4 stroke engine)/ 1(for 2 stroke engine).

The longer fuel-injection duration is due to the injection of a higher fuel quantity of biodiesel because of its lower LHV compared to mineral diesel. A higher combustion efficiency with biodiesel (Figure 5) is unable to compensate for the lower LHV and lower BTE of biodiesel. For biodiesel, the injection needle starts to rise earlier and closes later for all notches (Figure 16). The maximum needle lift is also higher for biodiesel due to higher injection pressures. A higher bulk modulus of compressibility for biodiesel results in a higher speed of sound in the test fuel. With in-line, PLN-type fuel-injection systems, this leads to a rapid transfer of pressure waves from the fuel pump to the injector needle, leading to an earlier needle lift (appendix 1, Table 7). Choi et al.[39] attributed the change in fuel-injection timing to the higher viscosity of biodiesel. The viscosity directly influences the amount of fuel that leaks past the plunger in the fuel pump and the needle. Higher viscosity biodiesel leads to reduced fuel losses during the injection, leading to a faster evolution of pressure, therefore advanced fuel-injection timings.

The in-cylinder pressure -CAD diagram for the test fuels (Figure 17) at different notches is analyzed for evaluation of combustion behavior. Details about the in-cylinder pressure data processing are given in appendix 2. An oscillatory nature of in-cylinder pressure rise at all notches is observed. With biodiesel, the frequency and amplitude of oscillations is marginally lower than that for mineral diesel, however, this difference is not significant. An earlier pressure rise is seen with biodiesel at all notches. Table 6 summarizes the timings of start of pressure rise.

No significant difference is seen in the peak in-cylinder pressure between various fuels at the eighth and the fifth notch. At idle notch however, B50 shows the highest peak in-cylinder pressures. The rate of pressure rise ($dp/d\theta$) curves confirm the oscillatory nature of the pressure in-cylinder (Figure 18). At each notch, biodiesel shows an earlier in-cylinder pressure rise, suggesting earlier heat release. This earlier rise of in-cylinder pressure for biodiesel is also supported and verified by an earlier SOI as compared to mineral diesel (Figures 9 and 16).

In addition, the SOC is earlier for biodiesel compared to mineral diesel at most notches (Figure 14). Figure 19 shows the heat-release rate for all test fuels, which also confirms the oscillatory nature of the combustion. At the eighth notch, two phases of premixed combustion are followed by mixing-controlled combustion. At the fifth notch, only one phase of premixed combustion can be observed, whereas at the idle notch, only premixed combustion is observed. At lower notches, combustion is mainly premixed because during ID, smaller fuel quantity is injected, which vaporizes and mixes well during the ID period due to longer time availability.

Earlier SOI for biodiesel is partially responsible for advanced heat release at all notches. Another reason is the presence of oxygen in biodiesel's molecular structure.

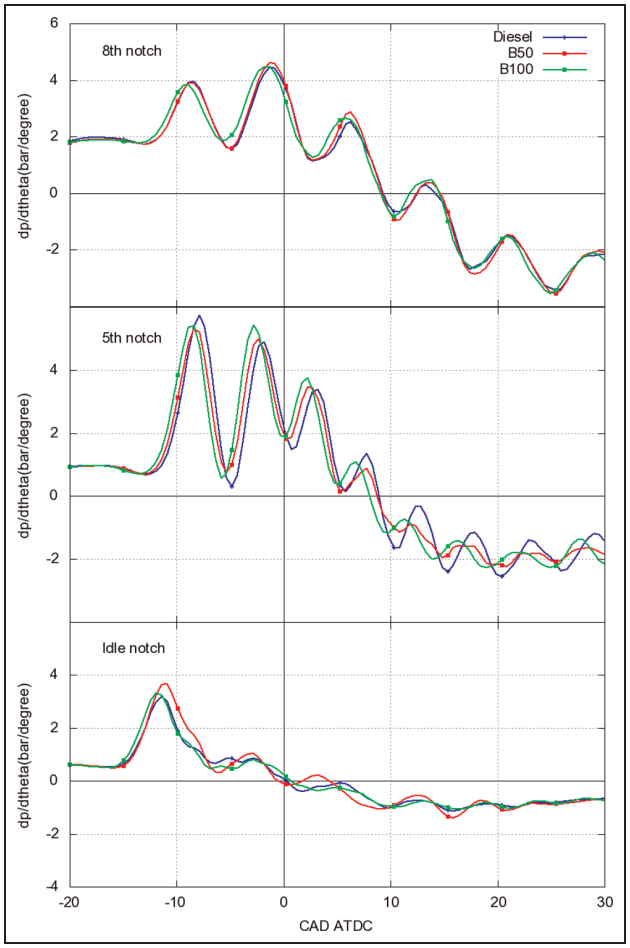

Figure 18. Rate of pressure rise for various test fuels.

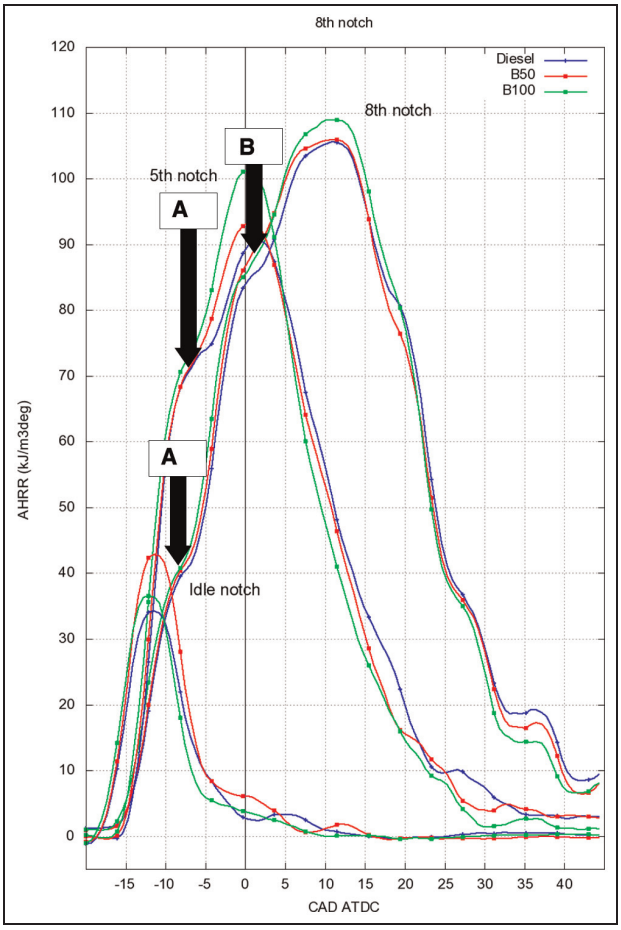

Figure 19. Heat-release rate (HRR) for various test fuels. A: end of first phase of premixed combustion; B: end of second phase of premixed combustion.

Szybist et al.[28] studied the ignition behavior of different fuels including biodiesel surrogate (methyl decanoate) in a cooperative fuel research (CFR) (CI) engine and reported that methyl decanoate exhibits a larger amount of low temperature heat release (LTHR) compared to mineral diesel. This raises the temperature of the combustible mixture by 200–300 °C, which may be responsible for earlier high-temperature heat release for biodiesel. LTHR cannot be prominently noticed in the heat-release diagram (Figure 19) possibly because of multiple hole injectors and averaging of the data. Maximum heat-release rates are given by B100 at the eighth and fifth notch and B50 at the idle notch. At the eighth notch, the phasing of the maximum heat-release rate of mineral diesel and biodiesel are similar; however, at this notch, there is an overlap of premixed and mixing-controlled combustion, and correct phasing may be obscured due to this overlap. At the fifth notch, maximum heat release of biodiesel is advanced and is closer to TDC compared to mineral diesel and B50. At the idle notch also, the maximum heat-release rate of biodiesel occurs earlier than mineral diesel. The P–θ diagram (Figure 17) shows that combustion is not optimized, as is also evident from the large oscillations. This has also been corroborated by a separate study revealing high combustion noise from this engine, which were not found to be the piping oscillations.

Premixed combustion is limited by the chemical reaction rate. As chemical reactions become mixing controlled, time scales for fuel spray/cylinder gas interactions differ by an order of magnitude from the time scales of the branching reactions. Hence, reaction rates of mixing-controlled combustion are relatively lower compared to reaction rates of premixed combustion.[40] In the mixing-controlled combustion, chemical reactions occur under higher local temperatures at 'flash spots' with local A/F ratios close to stoichiometric. With mineral diesel, there is relatively higher mixing-controlled combustion compared to biodiesel. For biodiesel, the O/C ratio at the flame lift-off length of the spray (due to presence of oxygen in biodiesel molecules, and due to a longer flame lift-off length itself) leads to higher ς_{st}% of stoichiometric air required for combustion of the entire fuel mass.[40] The parameter ς_{st} shows the percent of stoichiometric air entrained at the location of the flame lift-off length. Lift-off length is the anchoring point of the flame, as shown by Dec.[41] This results in higher premixed combustion, which correlates well with lower soot obtained from biodiesel.[32–36] The extent of air entrainment up to the lift-off point is important in establishing the local air–fuel ratio for premixed combustion and for subsequent reactions. Another noteworthy aspect

in Figure 17 is similarity in the pressure curves for the test fuels. This indicates that the large-bore quiescent-chamber medium-speed locomotive engine shows identical combustion behavior for the two fuels. This is in favor of biodiesel, as the polar diagram and the designs of various critical components and engine block are dependent to a large extent on in-cylinder pressure curves. Major modifications to the engine block and other critical power assembly components are therefore not required for the application of biodiesel in these locomotive engines.

Conclusions

The biodiesel was derived from cottonseed oil. With B100, the engine was able to develop a rated power identical to diesel; however, the BSFC of CME was 15% higher than mineral diesel. The BSFC of the engine increased as the biodiesel proportion in the test fuel increased. The BTE for biodiesel and blends was lower than that for mineral diesel; however, the difference was not as pronounced as for BSFC. The BTE at higher notches was comparable for mineral diesel and CME; B20 does not adversely affected the BTE, suggesting benefits of using B20 for large-scale implementation. Exhaust gas pressures before the turbine were generally higher for mineral diesel at lower notches, whereas B10 and B20 showed higher exhaust gas pressures at higher notches. Isentropic bulk modulus, speed of sound and density of the fuels have been calculated from the published data and it correlated well with measured SOI. Strong correlation between SOI and bulk modulus of compressibility has been established. Calculation of SOI based on injection equipment geometry confirmed the effect of these parameters in advancing the SOI for biodiesel.

The locomotive engine produced the highest $BSNO_x$ with B100 at higher notches. With B50, $BSNO_x$ emissions were 70–80% of maximum at lower notches; however, they were comparable to diesel at higher notches. The engine emitted the highest NO_x emissions (raw) at the third and fourth notches. PM emissions were highest for mineral diesel and reduced to 60% for B100. B50 produced the lowest BSHC emissions (10–40% of maximum) and diesel produced the highest BSHC emissions. BSCO and $BSCO_2$ emissions were highest for B100 and the lowest for mineral diesel. B100 showed relatively lower smoke opacity compared to mineral diesel at all notches. In this study, correlation between the NO_x and PM emissions with the O/C ratio of the fuel–air mixture has been established. For the same O/C ratio, B100 gave a mixed trend of NO_x emissions (lower NO_x at lower BMEP and higher NO_x at higher BMEP) and considerably lower particulates. Timings of peak in-cylinder mean gas temperatures and maximum heat-release rate were calculated, and these correlate well with NO_x emissions.

The fuel-injection pressures with biodiesel were higher than mineral diesel due to biodiesel's higher bulk modulus. Fuel-injection duration for biodiesel was 3–4 CAD higher than mineral diesel at the eighth notch. Experiments showed that the ID with biodiesel was relatively lower at lower and higher notches. It became relatively higher at intermediate notches. This was due to lower A/F and O/C ratios at intermediate notches. This was in addition to earlier 'start-of-combustion' as well as shorter 'combustion duration' of B100 compared to mineral diesel and heat release being advanced for biodiesel compared to mineral diesel. The above findings advanced the understanding of biodiesel combustion in locomotive engines.

References

1. Umer R, Farooq A and Gerhard K. Evaluation of biodiesel obtained from cottonseed oil. *Fuel Process Tech* 2009; 90: 1157–1163.
2. Nabi MN, Rahman MM and Akhter MS. Biodiesel from cottonseed oil and its effect on engine performance and exhaust emissions. *Appl Thermal Eng* 2009; 29: 2265–2270.
3. Rakopoulos CD, Rakopoulos DC, Hountalas DT, et al. Performance and emissions of bus engine using blends of diesel fuel with bio-diesel of sunflower or cottonseed oils derived from Greek feedstock. *Fuel* 2008; 87: 147–157.
4. Agarwal AK and Dhar A. Performance, emission and combustion characteristics of Jatropha oil blends in a direct injection CI engine. SAE paper 2009-01-0947, 2009.
5. Ben M, Terry CR and Simonton JL. Economic analysis and feasibility of cottonseed oil as a biodiesel feedstock. Final Report Project No. 1316-C059, Center for Engineering Logistics and Distribution Industrial Engineering Department, Texas Tech University, 2008.
6. Capareda SC, Powell J and Parnell C. Engine performance and exhaust emissions of cottonseed oil biodiesel. In: *2008 beltwide cotton conferences*, Nashville, TN, January 2008.
7. Savvidis D, Grammatikis V, Trandafyllis J, et al. Measuring the performance and the environmental effects of four-stroke diesel engines operated on the same plant oil methyl ester mixtures in two laboratories. SAE paper 2007-01-2022, 2007.
8. Savvidis D, Traindafyllis J, Grammatikis V, et al. Influence of various blends cottonseed methyl ester biodiesel on steady state emissions using an old technology Ford Escort on a chassis dynamometer. SAE paper 2007-01-4062, 2007.
9. National Cottonseed Products Association. Cottonseed oil, http://www.cottonseed.com/publications/csobro.asp.
10. McCormick RL, Graboski MS, Alleman TL, et al. Impact of biodiesel source material and chemical structure on emissions of criteria pollutants from a heavy duty engine. *Environ Sci Technol* 2001; 35: 1742–1747.
11. US Environmental Protection Agency. Title 40 - Protection of environment code of federal regulations part 92: control of air pollution from locomotives and locomotive engines.
12. Frey HC, Choi HW and Kim K. Measurement of the energy use and emissions of passenger rail locomotives using a portable emission measurement system. In: *Proceedings of 102nd annual conference and exhibition Air*

and Waste Management Association, Detroit, MI, June 2009, paper 2009-A-243-AWMA.
13. Assanis DN, Poola RB, Sekar R, et al. Study of using oxygen-enriched combustion air for locomotive diesel engines. *J Eng Gas Turbine Power* 2001; 121(1): 157–166.
14. Poola RB and Sekar R. Reduction of NO_x and particulate emissions by using oxygen-enriched combustion air in a locomotive diesel engine. *J Eng Gas Turbine Power* 2003; 125(2): 524–533.
15. Chen G, Flynn PL, Gallagher SM, et al. Development of the low-emission GE-7FDL high-power medium-speed locomotive diesel engine. *J Eng Gas Turbine Power* 2003; 125(2): 505–512.
16. Nerheim LM, An J, Liang S, et al. Development of the DLoco DL240ZJ engine to comply with current and future emissions regulations. In: *CIMAC congress*, Vienna, 2007.
17. Fritz SG. Evaluation of biodiesel fuel in an EMDG P38-2 locomotive. NREL Report No. NREL/SR-510-33416.
18. Miyamoto N, Ogawa H, Nurun N, et al. Smokeless low NO_x high thermal efficiency and low noise diesel combustion with oxygenated agents as main fuel. SAE paper 980506, 1998.
19. Siebers D and Higgins B. Flame lift-off on direct-injection diesel sprays under quiescent conditions. SAE paper 2001-01-0530, 2001.
20. Flynn PF, Durrett RP, Hunter GL, et al. Diesel combustion: an integrated view combining laser diagnostics, chemical kinetics and empirical validation. SAE paper 1999-01-0509, 1999.
21. Szybist J, Boehman AL, Haworth DC, et al. H. Premixed ignition behavior of alternative diesel fuel-relevant compounds in a motored engine experiment. *Combust Flame* 2007; 149: 112–128.
22. Heywood JB. *Internal combustion engine fundamentals*. New York: McGraw Hill Book Co., 1988.
23. Agarwal D, Sinha S and Agarwal AK. Experimental investigation of control of NO_x emissions in biodiesel-fueled compression ignition engine. *Ren Energy* 2006; 31: 2356–2369.
24. Mazumdar B and Agarwal AK. Performance emission and combustion characteristics of biodiesel (waste cooking oil methyl ester) fueled IDI diesel engine. SAE paper 2008-01-1384, 2008.
25. Kousoulidou M, Fontaras G, Ntziachristos L, et al. Biodiesel blend effects on common-rail diesel combustion and emissions. *Fuel* 2010; 89: 3442–3449.
26. Song JT and Zhang CH. An experimental study on the performance and exhaust emissions of a diesel engine fuelled with soybean oil methyl ester. *J Automobile Eng* 2008; 222(12): 2487–2496.
27. Herbinet O, Pitz WJ and Westbrook CK. Detailed chemical kinetic oxidation mechanism for a biodiesel surrogate. *Combust Flame* 2008; 154(3): 507–528.
28. Szybist J, Boehman AL, Haworth DC, et al. Premixed ignition behavior of alternative diesel fuel-relevant compounds in a motored engine experiment. *Combust Flame* 2007; 149: 112–128.
29. McCormick RL, Graboski M, Alleman TL, et al. Impact of biodiesel source material and chemical structure on emissions of criteria pollutants from a heavy-duty engine. *Environment Sci Tech* 2001; 35(9): 1742–1747.
30. Szybist JP, Boehman AL, Taylor JD, et al. Evaluation of formulation strategies to eliminate the biodiesel NO_x effect. *Fuel Process Tech* 2005; 86: 1109–1126.
31. Vioculescu IA and Borman GL. An experimental study of diesel engine cylinder averaged NO_x histories. SAE paper 780228, 1978.
32. Siebers D and Higgins B. Flame lift-off on direct-injection diesel sprays under quiescent conditions. SAE paper 2001-01-0530, 2001.
33. Flynn PF, Durrett RP, Hunter GL, et al. Diesel combustion: an integrated view combining laser diagnostics, chemical kinetics and empirical validation. SAE paper 1999-01-0509, 1999.
34. Graboski MS and McCormick RL. Combustion of fat and vegetable oil derived fuels in diesel engines. *Prog Energy Combust Sci* 1998; 24: 125–164.
35. Siebers DL. Scaling liquid-phase fuel penetration in diesel sprays based on mixing-limited vaporization. SAE paper 1999-01-0528, 1999.
36. Cardone M, Prati MV, Rocco V, et al. A comparative analysis of combustion process in d.i. diesel engine fueled with biodiesel and diesel fuel. SAE paper 2000-01-0691, 2000.
37. Sinha S and Agarwal AK. Experimental investigation of the combustion characteristics of a biodiesel (rice-bran oil methyl ester)-fuelled direct-injection transportation diesel engine. *J Automobile Eng* 2007; 221(8): 921–932.
38. Takaaki K, Takayuki I, Jiro S, et al. Detailed chemical kinetic modeling of diesel spray combustion with oxygenated fuels. SAE paper 2001-01-1262, 2001.
39. Choi CY, Bower GR and Reitz RD. Effect of biodiesel blended fuels and multiple injections on DI diesel engines. SAE paper 970218, 1997.
40. Higgins B, Siebers D and Aradi A. Diesel-spray ignition and pre-mixed burn behavior. SAE paper 2000-01-0940, 2000.
41. Dec J. A conceptual model of DI diesel combustion based on laser-sheet imaging. SAE paper 970873, 1997.
42. Luthra SK. Development of fuel injection systems for diesel engines with dynamically varying timings. In: *IXth national conference on IC engines and combustion IIP*, Dehradun, India, 1985.
43. Hwang NHC and Houghtalen RJ. *Fundamentals of hydraulic engineering systems*. 3rd ed. Prentice Hall Inc., 1996.
44. Tat ME and Van Gerpen JH. Measurement of biodiesel speed of sound and its impact on injection timing. NREL Report No. NREL/SR-510-31462, 2003.
45. Arcoumanis CM, Gavaises YM and Oiwa J. Application of a FIE computer model to an in-line pump-based injection system for diesel engines. SAE paper 970348, 1997.
46. Boehman AL, Morris D and Szybist J. The impact of the bulk modulus of diesel fuels on fuel injection timing. *Energy Fuels* 2004; 18(6): 1877–1882.

Appendix 1: Ignition Delay Calculations

The governing equation showing dependence of injection delay on the velocity of sound is[42]

$$\theta_{injd} = (6N * L)/V_o \text{CAD} \quad (4)$$

Here, N is the rotational speed of the engine (r/min), L is the length of the high-pressure tubing (m) and V_o is the velocity of the pressure wave in the high-pressure tubing (m/s). This equation is clearly speed dependent, and would be the same for all speeds if expressed in

time units. The equation assumes constant injection pressure and is independent on the plunger diameter.

V_o, the velocity of the pressure wave, is given by (because the port is closed abruptly) Hwang and Houghtalen[43]

$$V_o = \sqrt{\frac{E}{\rho}} \tag{5}$$

where $\frac{1}{E} = \frac{1}{E_f} + \frac{D}{wE_p}$, D is the inside diameter of the pipe, E is the composite elastic modulus, E_f is the elastic modulus of the fuel, E_p is the elastic modulus of the pipe material, w is the pipe wall thickness and ρ is the fuel density.

In order to compare the effect of density and bulk modulus on the speed of sound in the fuel (and on the velocity of the propagating wave), the bulk modulus of CME was calculated from published data. Tat and Van Gerpen[44] provided measured values of the speed of sound and the bulk modulus of different esters and mineral diesel. The bulk modulus for CME was calculated from the measured values of different methyl esters from this report. A simple weightage formula was used to account for the effect of the bulk modulus of different constituents of CME

$$E_{CME} = \sum E_i w_i \tag{6}$$

where E_{CME} is the bulk modulus of compressibility of CME, E_i is the bulk modulus of compressibility of the component methyl ester calculated at 40 °C and 6 bar, which are the temperature and pressure of the CME just before port closing and w_i is the weight in percentage of the component methyl ester. The speed of sound was calculated in a similar manner as given above. The density, bulk modulus of compressibility and the speed of sound of mineral diesel and the CME as calculated are shown in Table 7.

The bulk modulus of compressibility of biodiesel is higher than diesel, hence, an earlier SOI for biodiesel is observed. The effect of density is less pronounced than the bulk modulus of compressibility. Arcoumanis et al.[45] carried out a study on relative effects of the bulk modulus of compressibility of fuel and its density on the fuel-injection timing in a diesel engine. They reported advanced fuel-injection timing by 0.5 CAD for an increase in the bulk modulus of less than 15%. In comparison, similar changes in the liquid density had little effect on the fuel-injection timings. Boehman et al.[46] confirmed that the higher bulk modulus of compressibility of vegetable oils and their methyl esters led to advanced injection timing with in-line PLN fuel-injection systems.

In the present study, 11% increase in the bulk modulus of compressibility of CME has resulted in an advance of 0.93 CAD in SOI over diesel. A rough calculation of the impact of the speed of sound on the fuel-injection timing has been assessed as follows. The length of the high-pressure tube from the fuel-injection pump to the injector nozzle is 0.56 m, and there is an additional 0.2 m drilled passage in the injector nozzle holder. For diesel, the pressure wave will take 0.581 ms to travel through the tube, and for CME, it will take 0.565 ms, which results in 0.1 CAD earlier SOI for CME. To study the effect of bulk modulus, the following formula developed by Tat and Van Gerpen[44] can be used

$$\theta = \frac{(\mathrm{NOP} - P_0)V_f}{BV_\theta A_p} \tag{7}$$

Here, θ is the CAD for opening of the injector needle, NOP is the nozzle opening pressure, P_0 is the initial system pressure, V_f is the volume of compressed fuel, B is the isentropic bulk modulus, V_θ is the plunger velocity and A_p is the plunger area. θ for diesel is calculated as 1.9 CAD, and for biodiesel, it is 1.6 CAD.

Appendix 2: Cylinder Pressure Calculations

Averaged cylinder pressure data has been smoothened using a low-pass mean value filter. Signal smoothening has been carried out with the floating mean procedure. Each value has been calculated from the linear value of the adjacent values to the left and right. The number of adjacent values (per side) represents the order, and an order of 3 has been used to smooth the pressure signal in the present case.

$$y_{TM}(i) = \frac{1}{1+2n}\sum_{i-n}^{i+n} y(i) \tag{8}$$

Here, i is the current abscissa and n is the order.

For calculation of heat release, a simplified process has been used, and surface losses have been ignored. The curve of polytropic coefficient is taken into account in relation to temperature by an approximation formula. The gas mass has been calculated by determination of temperature. The gas mass has been calculated

Table 7. Correlation of fuel properties to injection timing.

Fuel	Isentropic bulk modulus (MPa)	Speed of sound (m/s)	Density (g/cm^3) at 40 °C, 6 bar	SOI CAD at eighth notch (1050 r/min)
Diesel	1408.3	1308.6	0.8275	−18.06
CME	1564	1344.8	0.8673	−18.99
Variation from diesel	+ 11%	+ 2.8%	+ 4.8%	0.93 CAD advanced

from the intake manifold pressure, intake manifold temperature and volumetric efficiency.

$$m = Im_{th} = IV_H\rho = IV_H\frac{p_s}{RT_s} \tag{9}$$

Here, I is the volumetric efficiency, m_{th} is theoretical mass, ϱ is the gas density, V_H is the swept volume, p_s is the intake manifold pressure, R is the universal gas constant (287.12 kJ/kgK) and T_s is the intake manifold temperature.

$$Q_i = \frac{c}{\kappa_{i-1}}V_{i+n}\left[p_{i+n} - p_{i-n}\left(\frac{V_{i-n}}{V_{i+n}}\right)^{\kappa_i}\right](X_i + 1) \tag{10}$$

Here, Q_i is the instantaneous heat release, κ_i is the polytropic coefficient, C_{Vi} is the specific heat at constant volume, T_i is temperature, Xi is the mass fraction, n is the interval (1°) and c is a constant.

$$\begin{aligned}
\kappa_i &= \frac{0.2888}{C_{Vi}} + 1\\
C_{Vi} &= 0.7 + T_i(0.155 + A_i)10^{-3}\\
A_i &= 2X_i\\
X_i &= \frac{\sum Q_i.28}{p_s}\\
T_i &= \frac{V_i p_i}{mR}
\end{aligned} \tag{11}$$